# Stage-discharge relationship in tidal channels

William S. Kearney[1]

Giulio Mariotti[2]

Linda A. Deegan[3]

Sergio Fagherazzi[1]

1. Department of Earth and Environment and Marine Program, Boston University, Boston, MA, USA

2. Department of Oceanography and Coastal Sciences, Louisiana State University, Baton Rouge, LA, USA

3. The Ecosystems Center, Marine Biological Laboratory, Woods Hole, MA, USA; Now at Woods Hole Research Center, Falmouth, MA, USA

Corresponding author: William Kearney, Department of Earth and Environment, 685 Commonwealth Avenue, RM 130, Boston, MA 02215

Running head: Tidal stage-discharge relationship

Keywords: Tidal hydrodynamics, discharge measurements, rating curve, time series, salt marsh channels

# Abstract

Long-term records of the flow of water through tidal channels are essential to constrain the budgets of sediments and biogeochemical compounds in salt marshes. Statistical models which relate discharge to water level allow the estimation of such records from more easily obtained records of water stage in the channel. Here we compare four different types of stage-discharge models, each of which captures different characteristics of the stage-discharge relationship. We estimate and validate each of these models on a two-month long time series of stage and discharge obtained with an Acoustic Doppler Current Profiler in a salt marsh channel. We find that the best performance is obtained by models that account for the nonlinear and time-varying nature of the stage-discharge relationship. Good performance can also be obtained from a simplified version of these models, which captures nonlinearity and nonstationarity without the complexity of the fully nonlinear or time-varying models.


# Introduction

The flow of water into and out of tidal channels carries with it nutrients, sediment and biota thus exerting a strong control on the biology and geomorphology of environments such as mudflats, mangroves and salt marshes (Morris et al. 2002; Chmura et al. 2003; Duarte et al. 2005; Cai 2011; Fagherazzi et al. 2013). Accurately estimating the volumetric flux of water, or discharge, through a channel is a crucial component of estimating the flux of materials transported through these systems. The flux of an advected material is equal to its concentration multiplied by the discharge. Precise

estimates of discharge are therefore important to quantify the exchange of biogeochemical compounds between marshes and nearby bays (Carey and Fulweiler 2014) and determine the stability of salt marshes from channel sediment fluxes (Ganju et al. 2013, 2015).

Discharge can readily be measured in tidal channels with a towed acoustic Doppler current profiler (ADCP) survey (Ruhl and Simpson 2005; Mueller et al. 2009), but such surveys are labor-intensive and do not provide the long time series of discharge which are necessary to capture low-frequency variability and the effects of storms. Such time series can be developed from deployments of bottom-mounted upward-looking ADCPs, properly calibrated to the true discharge through the channel. If one is interested, however, in understanding the stability of tidal wetlands from their sediment budgets (Ganju et al. 2013, 2015), one might like to instrument simultaneously dozens of channels in marshes in a wide variety of geomorphic and hydrological settings. The expense of ADCPs becomes prohibitive at these scales. Stage-discharge models allow one to estimate discharge using measurements from an independent water level logger, an instrument much more cost-effective to deploy at scale.

The development of rating curves, which relate the easily measured water level, or stage, in a stream cross section to the flow through that cross section, is routinely carried out in rivers (Kennedy 1984). Once a rating curve is constructed, discharge can be instantaneously estimated by measuring water level. In coastal streams influenced by tides, simple models for rating curves (such as power laws) fail because of the bidirectional and nonstationary nature of flow in these environments. Bidirectionality means that, in one tidal cycle, there are two discharges with opposite signs for a given

stage. Moreover, tidal asymmetry (Boon 1975; Pethick 1980; Healey et al. 1981; Fagherazzi et al. 2008) means these discharges display a hysteresis between ebb and flood—the ebb discharge is not simply the time-reversed flood discharge. Nonstationarity in tidal channel flow means that a single water level corresponds to many different discharges over the course of a stage-discharge record. This nonstationarity arises from tides amplified by storm events and from lower-frequency harmonics of the tide such as the spring-neap cycle. Bidirectionality, hysteresis and nonstationarity confound attempts to estimate an instantaneous rating curve for tidal systems.

Here, we examine a suite of models for estimating discharge from stage measurements. We explore the structure of each of these models and their relation to our physical understanding of flow in tidal systems and discuss the challenges to estimating the parameters of each model from stage and discharge data. We present a case study using stage-discharge records from a salt marsh creek along the Rowley River, Massachusetts, USA, to compare the performance of each of these methods. We conclude by discussing the advantages of each model and our recommendations for stage-discharge modelling in tidal creeks.

# Procedures

### Discharge measurements

A data set associating discharge with creek stage was acquired over two thirty-day deployments in August and September 2015 in a salt marsh creek (Sweeney Creek) along the Rowley River, MA. The measurement location is just after the confluence of two first-order channels (Fig. 1), though there has been extensive ditching of the Sweeney

Creek marsh. The marsh surface is vegetated by *Spartina patens* with *S. alterniflora* along the creek banks. The tidal range at the site is just over 2 m and the channel drains nearly completely at low tide. The channel is asymmetric, with the thalweg of the creek closer to the right bank (looking towards the Rowley River, downstream on ebb tide), and the right bank consists of a step, vegetated with *S. alterniflora* before rising to the *S. patens* dominated platform.

A Nortek Aquadopp acoustic Doppler current profiler (ADCP) operating at 2.0 MHz was programmed to record velocities in 20 cm bins at 10-minute intervals. The blanking distance of the ADCP was set to 10 cm, so that the center of the first bin is 20 cm above the ADCP (Table 1). The ADCP was installed looking upward in the creek thalweg. The velocity data retrieved from the ADCP consist of three BxN matrices where B is the number of bins and N is the number of points recorded in time. Each of the three matrices represents velocity in one of three directions (east, north and up, ENU). In addition, the water pressure recorded by the ADCP is retrieved. This pressure is converted to a height of water above the ADCP by dividing by the specific weight of water. The velocity data are filtered to remove velocities recorded in bins above the water level and then the filtered velocities are averaged to provide a trivariate time series of average velocity above the ADCP in each of the three directions. The ENU velocity time series must be rotated to extract the along-channel velocity, which will serve as the index velocity in the cross section. The variability in velocity in a long channel driven by the tides is dominated by the along-channel flow. Principal components analysis resolves this dominant axis of variability, rotating the velocity into three principal components in the

along-channel, across-channel and vertical directions (Fig. 2a). Choosing the first principal component of the rotated data set provides a time series of index velocity.

A channel cross section was measured on foot by RTK-GPS (Topcon HIPER-V; Fig. 1b) with sub-centimeter accuracy in the horizontal and vertical dimensions. The stage measurements from a pressure transducer in the ADCP along with the GPS cross section were used to calculate the flooded cross-sectional area. The index discharge is calculated by multiplying this area by the index velocity. Calibration of the index discharge to the true discharge through the channel is essential for any consistent estimate of material flux in the channel (Ruhl and Simpson 2005). Two index discharge calibrations were performed at the Sweeney Creek cross section using two different methods. The first, recorded during the second ADCP deployment in September 2015, used a handheld flow meter (Marsh-McBirney Flo-Mate 2000) to sample velocities at stations spaced every 1 meter across the channel. Two or three velocity measurements were taken at each station following the two-point method (measurements at 20% and 80% of the total depth) for water levels under 150 cm and the three-point method (measurements at 20%, 60% and 80% of the total depth) for water levels above 150 cm. The velocity measurements at each station were averaged and then multiplied by the area of the station (1 m times the water level) to determine discharge through that station. The true discharge in the channel is the sum of discharges at each station. Measurements were recorded every thirty minutes for an entire tidal cycle. A second calibration was carried out in September 2016 at the same cross-section using a tow-across ADCP (Teledyne RD Instruments StreamPro ADCP) following the procedures in Mueller and Wagner (Mueller et al. 2009). Four transects of the channel were performed every ten minutes for an entire tidal cycle, and

the four measurements were averaged together to estimate the discharge at ten minute intervals. A linear regression from the index discharge to the true discharge (Ruhl and Simpson 2005) was calculated using the data from both calibration methods simultaneously and then applied to the entire index discharge time series to obtain a true discharge time series. This approach resulted in two time series—one of true discharge and one of stage—for each of the two deployments of the ADCP.

**Modeling of the discharge**

We examine four different classes of model: a geometric model of flow proposed Boon (1975), a linear, time-invariant model inspired by the unit hydrograph formulation of flow in rivers (the TIGER model presented in Fagherazzi et al. 2008), a nonlinear, time-invariant model based on the Volterra series (Rugh 1981), and a new linear, time-variant model inspired by the recent interest in time-variable travel time distributions (Fagherazzi et al. 2008; Botter et al. 2010; Harman 2015; Beven and Davies 2015). Below, we briefly describe the models we estimate on our stage-discharge time series. More detail on each model and on the procedures used to estimate the parameters of these models can be found in the supplemental materials.

Throughout, we use the notation Q(t) to represent the time-varying discharge in a cross section and h(t) the time-varying stage in that cross section, $\{Q_i\}_{i=0}^{N-1}$ and $\{h_i\}_{i=0}^{N-1}$ are the discrete stage-discharge time series of length N taken at a sampling interval of $\Delta t$ (i.e. $Q_i = Q(i\Delta t)$ and likewise for the stage).

**The Boon model**

Boon (1975) proposed a stage-discharge model as follows

(1) $Q(t) = A(h)\frac{dh}{dt}$

where A(h) represents the hypsometric curve, the distribution of area within the salt marsh as a function of height. This model can be derived from the continuity of mass under the assumption that water surface slopes are negligible throughout the marsh. If adequate topographic data is available, the hypsometric curve can be estimated (Boon 1975). In the absence of those data, a representation of the hypsometric curve can be estimated from the stage-discharge data. We assume a power law form for the hypsometric curve, $A(h) = \alpha h^{\beta}$ . We approximate $dh/dt$ by the backward difference operator: $dh/dt\big|_{t=i\Delta t} \approx (h_i - h_{i-1})/\Delta t$ . These assumptions lead to a nonlinear system of equations in the parameters $\alpha$ and $\beta$ of the form

(2) $Q_i = \alpha h_i^{\beta}(h_i - h_{i-1})$

for $i \in \{2,..,n\}$ which we solve for the optimal values of $\alpha$ and $\beta$ using nonlinear least squares with the Nelder-Mead method (Kelley 1999).

Extensions of Boon's model have been studied by Pethick (1980), who proposed, based on simple models of channel geometry, theoretical forms of $A(h)$ which are encompassed by the power law model we use here.

**Linear, time-invariant models**

The Boon model is a first-order approximation to flow in small tidal systems which captures the large-scale behavior of the flow (Fagherazzi 2002; Fagherazzi et al. 2003).

However, the assumption in the Boon model that water surface slopes are negligible has been pointed out as unrealistic, particularly on the ebb tide and as the tide rises over the channel banks and flows onto the marsh surface (Healey et al. 1981; Fagherazzi et al. 2008), and the model also requires an asymmetric tide to generate asymmetric discharges (Pethick 1980). More fundamentally, the Boon model assumes that the tide propagates instantaneously into the marsh. Instantaneous propagation forces the discharge to be in phase with the rate of change in stage even though lags between the peak discharge and the maximum rate of change in stage are observed in many tidal channels (Myrick and Leopold 1963; Bayliss-Smith et al. 1979). Fagherazzi et al. (2008) put forward a model based on the instantaneous unit hydrograph developed for river runoff which relaxes this assumption, assuming that the tidal propagation can be described by a travel time distribution $p(t)$ which determines how much of the flow at time $t$ is due to the increase in stage at time $t=0$. The tidal discharge is obtained by convolving this travel time distribution with the Boon model.

(3) $$Q(t)=\int_{-\infty}^{t} A(h)\left.\frac{dh}{dt}\right|_{t=\tau} p_h(t-\tau)\,d\tau$$

Because of the dependence of the hypsometric curve $A(h)$ and the travel time distribution on water stage, this formulation is naturally time-variant. We first consider a time-invariant version of this model ( $p_h(t)=p(t)$ for all $t>0$ ) which is both very simple to estimate and able to draw on the rich literature on system identification in linear, time-invariant systems

(4) $$Q(t)=\int_{-\infty}^{t} \left.\frac{dh}{dt}\right|_{t=\tau} \beta(t-\tau)\,d\tau$$

where we note that we have also incorporated the hypsometric curve into the time-invariant travel time distribution, averaging out its temporal variation to preserve the time-invariance of the model. In other words, we do not estimate a hypsometric curve explicitly in this or any of our later models. This integral equation can be discretized at our sampling frequency, which results in an overdetermined system of linear equations in the parameters, $\beta = \{\beta_i\}_{i=0}^{M-1}$ .

(5) $$Q_n = \sum_{i=0}^{M-1} \beta_i \left. \frac{dh}{dt} \right|_{t=(n-i)\Delta t}$$

Since we ultimately approximate the derivative by a backward difference, the linear model is equivalent to one with $dh/dt$ replaced by $h$ in Eq. 5 and the backward difference incorporated into the kernel coefficients, $\{\beta_i\}_{i=0}^{M-1}$ .

$M$ is the system order which determines how far back in time the discharge depends on stage. The system order is a hyperparameter of the problem, which needs to be selected before estimating the model parameters $\beta$ . We perform hyperparameter optimization for this and all models using cross-validation, explained below.

**Nonlinear, time-invariant models**

Frictional interactions between water, the banks of the channel and the marsh surface introduce nonlinearities into the continuity formulation (Speer and Aubrey 1985). Heterodyning of the stage signal by the nonlinear friction terms introduces higher frequency harmonics of the tide into the discharge, which helps explain the tidal discharge asymmetry (Speer and Aubrey 1985; Blanton et al. 2002). A linear model such as the system above is unable to account for this behavior and therefore cannot generate

frequencies in the output signal that are not present in the input signal. Rather the model only attenuates or amplifies the strength of the tidal signal at certain frequencies. We therefore investigate a nonlinear (but still time-invariant) model that is capable of generating these harmonics.

The canonical nonlinear equivalent to the linear, time-invariant system is the Volterra series, also seen in its orthogonalized version, the Wiener series. The Volterra series bears the same relationship to a linear, time-invariant system as a Taylor series does to the evaluation of a function at a point: it can be thought of as a Taylor series with memory. The Volterra series expands the system as a series of integrals of products of the stage signal at different lags

$$(6)\quad Q(t)=\sum_{k=0}^{K}\int_{-\infty}^{t}\cdots\int_{-\infty}^{t} f_k(t-\tau_{1,}..,t-\tau_k)\prod_{j=1}^{k} h(\tau_j)\,d\tau_j$$

so that the first few terms look like

$$(7)\quad Q(t)=f_0+\int_{-\infty}^{t} f_1(t-\tau_1)h(\tau_1)\,d\tau_1+\int_{-\infty}^{t}\int_{-\infty}^{t} f_2(t-\tau_{1,t}-\tau_2)h(\tau_1)h(\tau_2)\,d\tau_1\,d\tau_2+\cdots$$

Note that the first convolution in this series is simply the linear time-invariant system, and the n-th term in the series involves n-degree monomials of the stage at n different times in the past. We can likewise discretize the Volterra series, giving us a set of nonlinear equations in the coefficients (the discrete versions of the functions $f_k$ ). To estimate the coefficients effectively, we exploit the duality between the Volterra series and polynomial kernel regression (Franz and Schölkopf 2006).

**Linear time-variant models**

When water overtops the channel banks, discontinuities in the flow regime are observed (Bayliss-Smith et al. 1979), reflecting the activation of different flow mechanisms in these different regimes. Both the linear, time-invariant model and the Volterra series model estimate a single model for the entire time series, disregarding these changing flow regimes. This leads to underestimating the high magnitude discharges just before and after the high slack water and to overestimating the discharge at relatively low flows, which are dominated by residual drainage from the low-order creeks and ditches in the system and from seepage out of channel banks (Gardner 1975). Thus the TIGER model of Fagherazzi et al. (2008) and similar models developed for river basins (Botter et al. 2010; Harman 2015) explicitly account for time-varying travel time distributions. Estimating these travel time distributions is challenging because one needs to estimate both the distribution itself and the dynamics of the distribution as it changes in time. If one attempts to estimate a different travel-time distribution as in Eq. 5 for each point in the time series, then there is a sample size of one for each estimation problem and the problem is ill-posed.

We therefore have to approximate the dynamics of travel time distributions so they can be estimated with the finite amount of data that we have. We assume that there are a finite number of states that the flow can be in. We partition the time series into these states and estimate a linear, time-invariant travel time distribution for each state with only those data points representing these states. To predict discharge from a new stage trajectory, we assign the new trajectory to the appropriate state and use the linear model associated with that state to estimate the discharge.

We need to devise a principled way to partition the training data set into states and to assign a new, unobserved stage trajectory to a state. Here, for simplicity, an unsupervised clustering method (k-means; Xu and Wunsch 2009) partitions the $M$-dimensional training stage trajectories into $k$ clusters such that each trajectory belongs to the cluster with the closest mean in the Euclidean distance. Upon recording a new stage trajectory, we compute the distance from the new trajectory to each of the $k$ cluster centers, assign it to the cluster with the smallest distance and use the appropriate linear model to estimate discharge.

This unsupervised method uses only the information in the stage trajectories to form the clusters. It does not take into account the predictive performance of each cluster; this is not necessarily the optimal clustering for discharge estimation. One could, in principle, construct a clustering to optimize the estimation performance, but one would then need to model separately the process that assigns new stage trajectories to these clusters using a supervised classification technique. In practice, the unsupervised clustering performs well without this additional complication.

A further simplification can be made to the k-means-based, linear, time-variant model. The k-means clustering can be easily replaced by an ad hoc procedure that extracts four clusters simply using local information on the stage and stage derivative, making this approximation useful for real-time discharge estimation. The clusters are replaced by four states: high flood stages, low flood stages, high ebb stages and low ebb stages. The distinction between flood and ebb tides can be found where the time derivative of stage (approximated with the backward difference) changes sign. It is positive on the flood tides and negative on the ebb tides. The distinction between high and low stages can be

based on a threshold, which we choose by cross-validation. A stage trajectory is assigned to one of these four states by examining the stage and time derivative of stage at the time point to be estimated (the end of the trajectory). Otherwise, estimation of the linear models proceeds as in the k-means model.

**Regularization**

The individual stage measurements at each ten-minute interval are highly correlated with each other, so that each stage data point does not provide independent information for the discharge prediction. This is the collinearity problem familiar to users of multiple regression (Hocking 1976; Wold et al. 1984). When performing a straightforward regression with this collinear data, we will tend to overfit our model to the training data, reducing its ability to generalize to new data. We will also obtain unphysical estimates of the parameters that oscillate rapidly and are sensitive to noise. Regularization trades off fitting the training data set and constraining the parameters in some way. Variable selection by a stepwise procedure or model selection with the Akaike information criterion (Burnham and Anderson 2002) is one form of regularization. Here, we use Tikhonov regularization (also called ridge regression) which adds a penalty term to the least-squares objective function

(8) $$\hat{\beta} = \arg\min_{\beta} \sum_{i=1}^{N} \left(Q_i - H_i\beta\right)^2 + \left|\Gamma\beta\right|^2$$

where $\Gamma$ is some positive semi-definite matrix. The penalty term enforces some constraints on the structure of the coefficients, $\beta$, constraints chosen by the regularizing matrix $\Gamma$. For $\Gamma$ a multiple of the identity matrix, $\Gamma = \lambda I$, we obtain the common $L_2$ regularization which penalizes solutions with higher Euclidean

299 norms, leading to smooth parameter estimates where the degree of smoothness controlled
300 by the hyperparameter $\lambda$. Other choices of $\Gamma$ impose different constraints on the
301 system that may enhance the interpretability of the model. For example, stable spline
302 kernels (Pillonetto and De Nicolao 2010) enforce stability of a linear, time-invariant
303 system, leading to an appropriately decaying impulse response, while in kernel regression
304 methods such as that used to implement the Volterra series model, the matrix $\Gamma$
305 corresponds to the measurement error covariance, which could, in principle, be
306 independently estimated. However, we use $L_2$ regularization in our assessment below, as
307 it offers reasonable performance without much additional complexity.

308 **Cross-validation**

309 To estimate the hyperparameters of each model, such as the system order or the
310 regularization parameter, we use a cross-validation approach. We divide our training data
311 set evenly into two blocks, define a set of values of each hyperparameter to test, and
312 estimate the model with each possible combination of hyperparameters using only the
313 data from the first block. We apply the estimated model to the second half of the training
314 data set and measure the mean squared error between the estimated discharge and the
315 observed discharge in that block. We choose the values of the hyperparameters that
316 minimize this prediction mean squared error and re-estimate the model on the entire
317 training data set using these optimal hyperparameters before applying it to any further
318 stage records from the same creek.

319 **Discharge estimation with a fitted model**

To apply these models to the stage-discharge relationship for a particular channel, one must first collect a training data set with an ADCP and fit the model as described above. Thereafter, discharge can be estimated with only an independent water level logger instrumenting the channel. One records water level in the same cross section at the same sampling rate as the training data in the same cross section. Different cross sections will exhibit different stage-discharge relationships, and a model estimated on one cross-section is not valid at other cross sections within the same channel, let alone in different channels. The sampling rate must be identical because the each of the parameters in all of the models takes the form of a coefficient that is applied to stage a certain amount of time in the past. To estimate discharge at the present time, one collects the stage time series from the present stretching back into the past a certain amount of time. We call this short record a "stage trajectory." In our measurements, at time steps of 10 minutes each, a 25-hour-long stage trajectory is a vector of length 150. Each model takes a stage trajectory and applies some transformation to it—a linear combination of the stages in the linear, time-invariant model, for instance—and returns an estimate of discharge. If estimates of uncertainty are required for the estimated discharge value, bootstrap methods adapted for time series (Bühlmann 2002) can be easily applied to each of the models, though we will not specifically address methods for uncertainty quantification here.

# Assessment

To compare the performance of each of these models, we estimate each model on our ADCP stage-discharge records from the Rowley marshes. We follow the cross-validation procedure outlined above to estimate the parameters for each model on the first of the

two stage-discharge records and apply the model to the second ADCP record. We examine, in turn, the parameters estimated for each model, the estimation performance of each model on the second stage-discharge record, the behavior of the residuals, and the impact that regularization has on both the estimated parameters and the estimation performance.

**Model structure**

Each of the four classes of model uses a slightly different type of parameter set, and we show each of the resulting parameters in Fig. 3. The Boon model produces an estimated hypsometric curve in a power law form (Fig. 3a). The linear time-invariant model produces a single impulse response, representing the contribution of stage in the past to flow in the present (Fig. 3b). The Volterra series model generates a set of multidimensional impulse response functions. For simplicity, we show just the first order Volterra operator, which is just a linear, time-invariant impulse response, and the second order Volterra operator, which is a two-dimensional set of coefficients (Fig. 3c). The k-means model produces $k$ impulse responses, one for each of the clusters, and also assigns each point in the time series to one of these clusters (Fig. 3d).

The ideal system order in the linear models and the Volterra series describes how much memory is needed to estimate discharge effectively. Using cross-validation to select the system order ensures that we do not choose an order too large, in which case the model would overfit the data and have poor prediction performance on the validation data set. We find that, for the linear models, the optimal system order corresponds to approximately 25 hours or two full tidal cycles.

For the Volterra series, however, fewer lagged measurements of stage are required to predict the discharge, with an optimal system order around three hours. In estimating the Volterra series by a polynomial kernel regression, we exchange memory for degrees of nonlinearity as the number of parameters for each order of the Volterra operator scales as $N^m$ for a system order of $N$ and a Volterra operator order of $m$. Given our finite data set, we will be able to estimate only a finite total number of these parameters, so using a higher system order—a longer memory—forces the order of the Volterra series down. And indeed the optimal Volterra order for a three-hour system order is 5, corresponding to polynomials up to quintics, while that for a 25-hour system is 3, corresponding to cubic polynomials.

The k-means model uses an unsupervised method to determine which cluster a new stage trajectory belongs to, so that the clustering is determined entirely by the shape of the stage signal. Two given stage trajectories will be closest in the Euclidean metric when they are perfectly in phase and farthest apart when they are perfectly out of phase, so any unsupervised clustering method using the Euclidean metric will naturally cluster based on the phase of the tidal signal, as we find in Fig. 3d. For a system order of 25 hours, the optimal number of clusters is around four, corresponding roughly to a low flood tide, a high flood tide, a high ebb tide and a low ebb tide. We have found in practice, that the k-means clustering approach can be replaced by the thresholding procedure which extracts the four clusters mentioned above without significant loss of discharge estimation ability.

**Model performance**

For each of the models (Boon, LTI, Volterra, k-means), we use cross validation to estimate the model with good choices for hyperparameters. We re-estimate the model on the entire first time series using the good hyperparameters and apply each estimated model to our second stage-discharge time series and plot the modeled discharge values against the observed values in Fig. 4. The ideal modeled discharge values would lie on the red one-to-one line in Fig. 4. We report the Nash-Sutcliffe efficiency and the mean squared error of each model in Table 2 to compare the prediction performance of the four models.

The Volterra series model is the best performing (has the highest Nash-Sutcliffe efficiency and lowest mean squared error), followed by the k-means model, the Boon model and the linear, time-invariant model, a ranking which is supported by the visual representation of model fit, Fig. 4. Each of the four models tends to underestimate the high discharges and to overestimate the low discharges. At high magnitudes of the discharge, both positive and negative, points in Fig. 4 tend to lie on the side of the one-to-one line closer to the x-axis, while at smaller discharges, they tend to lie on the side further from the x-axis. This effect is more pronounced in the more poorly performing models (Boon and linear, time-invariant).

**Residual structure**

If our model completely captured the discharge-generating behavior of our salt marsh system, we would expect the residuals to be roughly independently distributed, in other words the error in the model comes not from systematically misestimating discharge at certain points of the time series but from random fluctuations in the velocity or from instrument noise. In addition to examining the fit of each model, we therefore also want

to examine the structure present in the residuals. The predictive capability of two models being equal, we prefer the one with the least correlation in the residuals, or, in the frequency domain, the model with the flattest spectrum. We plot the residual time series and power spectra for each of the four models in Fig. 5. While we observe some structure in the residuals, it is hard to determine visually which of the models whitens the residuals the best. We would like a quantitative measure of the residual structure. The Ljung-Box test (Ljung and Box 1978) provides a statistical test of the autocorrelation of the residual time series, but as we expect, the test rejects the null hypothesis of no autocorrelation for all of the models here, so the test itself does not adequately discriminate between the models. Instead, we use the spectral flatness (the ratio of the geometric mean of the power spectrum to the arithmetic mean) to measure how close to a white spectrum the residuals are. Flatness ranges from zero, at a signal with a single frequency, to one, at a purely white spectrum, so higher values of the spectral flatness indicate a better-specified model.

The estimated flatness of the residuals range from 0.021 for the linear, time-invariant model to 0.273 for the Volterra series model (Table 2). These values suggest that the Volterra series model is the best specified model of the four.

**Effect of regularization**

The unregularized linear, time-invariant impulse response is compared to that estimated with regularization in Fig. 6. We see that the effect of $L_2$ regularization is to smooth out the estimated coefficients. The main features of the response such as the high peak just after 100 lags (approximately 17 hours) are preserved in the regularized impulse response, but the finer scale oscillations are damped by the regularization. As the

regularization parameter $\lambda$ increases, lower and lower frequency oscillations are filtered out, and the resulting impulse response is smoother. Regularization improves the predictive ability of the linear, time-invariant model very slightly as measured by a larger out-of-sample Nash-Sutcliffe efficiency (from 0.640 to 0.646) and a smaller mean squared error (from 0.472 to 0.463).

The impact of regularization is much greater on the Volterra series model. The unregularized Volterra series parameters are a set of coefficients each corresponding to one of the data points in the training data set. The estimation procedure, as a result, is extremely sensitive to noise in the data—the Gram matrix of the polynomial kernel is ill-conditioned—and regularized as necessary to achieve any predictive ability with the model. When the fifth-order Volterra series model with 19 lags, the optimal model shown above, is estimated with no regularization ( $\lambda = 0$ ), the model is flatly unable to predict the discharge. The Nash-Sutcliffe efficiency is $-7 \times 10^{3}$ (note that negative Nash-Sutcliffe efficiencies correspond to models that predict the discharge worse than a constant model) while the mean squared error is $9 \times 10^{4}$ (the respective values for the regularized model are 0.980 and 0.025). Also notable is the stark increase in the variance of the parameters, from $3 \times 10^{-11}$ to $8 \times 10^{14}$ , and the correspondingly inflated discharge estimates, reaching as high as $200\, m^{3} \cdot s^{-1}$ . For such a high-dimensional regression problem, regularization is absolutely essential. With regularization, however, the Volterra series performs the best of the four models examined here.

# Discussion

**Physical realism and stage-discharge models**

453 The physical realism of each model roughly corresponds to its success in estimating the
454 discharge. The Boon and linear, time-invariant models both perform fairly poorly in all of
455 the measures examined (Table 2). The Boon model is derived from a continuity law and
456 is both nonlinear and nonstationary because of its dependence on the hypsometric curve.
457 However, it has long been recognized as incapable of matching the asymmetry and
458 hysteresis between flood and ebb tides because of its lack of memory. Only the slight
459 asymmetry of the stage on the ebb and flood tides enables a discharge asymmetry. The
460 linear, time-invariant model can generate asymmetry because it estimates discharge from
461 the history of the stage over the course of two full tidal cycles. It is therefore aware of
462 whether it is on a flood or an ebb tide and whether it is the higher or lower high tide of
463 the day. The linearity and, more importantly, the stationarity of this model are
464 nonphysical, and this lack of physical realism shows up in the performance of the model.
465 The linear, time-invariant model systematically underpredicts very high discharges and
466 overpredicts the low discharges because a single linear model is trained on the entire data
467 set. It essentially aims to interpolate between the high and the low discharges which
468 causes poor predictive performance on both.

469 The k-means model attempts to overcome this unphysical assumption of stationarity by
470 estimating several different models and switching between the models throughout the
471 tidal cycle. In doing so, it accounts somewhat for the nonlinearity problem as well. It
472 segments the high-dimensional space of the stage trajectories into $k$ Voronoi cells and
473 constructs a piecewise linear approximation to the nonlinear function which predicts
474 discharge from stage trajectories. The piecewise linear approximation should converge to
475 the true nonlinear function as the number of partitions increases, and the number of

partitions is here limited mostly by the amount of data available for training. As a result of this ability, it performs significantly better than the first two models. The Volterra series, while time-invariant and, like the linear, time-invariant model, unable to account for nonstationarity, captures naturally the nonlinearity present in the shallow water equations, which ultimately govern the system. The spectral flatness results show that this model is the best specified of the four. The Volterra series model is a parametric nonlinear system, but the duality between the Volterra series and polynomial kernel regression means we estimate the series with the latter, a nonparametric estimator of the system response. Because the kernel regression is nonparametric, it is not restricted by our misspecification and, with infinite training data and appropriate regularization to reduce the effect of noise, we should be able to converge on as close an approximation to the true system as is possible with a time-invariant model.

$L_2$ regularization is straightforward to implement, and for the discharge estimation problem, it is sufficient for estimating effective parameters. However, it does not necessarily lead to straightforwardly interpretable model coefficients. The impulse response of the linear, time-invariant model, for example, is a combination of the travel-time distribution, the hypsometric curve and the action of the time derivative, all of which are approximations because of the assumptions of linearity and time-invariance. A more sophisticated regularization scheme would take into account knowledge of the behavior of these parameters—such as the non-negativity and decaying tail of the travel-time distribution. If formulated carefully, these prior assumptions can be easily incorporated into the present regularization scheme by choosing an appropriate Tikhonov matrix (as in stable spline kernels (Pillonetto and De Nicolao 2010)). More complex prior assumptions

such as sparsity of the impulse response coefficients can not be handled with the quadratic penalty term of Tikhonov regularization, but other frameworks exist for these alternative forms of regularization (Tibshirani 1996; Zou and Hastie 2005; Aravkin et al. 2013) and in a Bayesian formulation of the estimation problem, characterizing our physical assumptions on the models by an arbitrary prior distribution is a type of regularization.

**Limitations of these models**

We have tested our models on stage-discharge records from a channel in a mesotidal salt marsh where the channel flow is almost entirely driven by regular tidal forcing. The models almost certainly do not work as well in environments with multiple drivers of flow such as microtidal channels with strong effects of wind on flow, tidally influenced streams with significant upland freshwater inputs, or loops in a channel network where the inputs and outputs do not flow through the same cross section. Future work will quantify which properties of our suite of models remain useful in other channels and what additional data might be necessary to extend this modeling framework to these other environments. While the models will not perform as well in these situations, their structure suggests that their relative performance will be similar; the k-means and Volterra series models are expected to perform better than the Boon and linear, time-invariant models because the structure of the former models is more flexible, and captures more complicated behavior than the latter models.

**Calibration**

The models presented here will estimate either the index discharge from the ADCP or the true discharge calibrated to cross-sectional discharge measurements, and they perform equally well on either task. We have here compared the modeled discharges against calibrated ADCP index discharges, which means our measures of model performance do not account for the uncertainty in the calibration. Proper calibration, is, however, essential to the estimation of material fluxes from these time series since the index discharge can vastly overestimate the water flux through the channel. The calibration requires a sizeable effort and appropriate instruments, and can also form a substantial part of the uncertainty of the discharge estimates, so it is important to stress the need for a good calibration. Several calibrations at a variety of tides can be done over the course of a single ADCP deployment, which collects the training data set for the stage-discharge model. Over the period in which one aims to estimate discharge from independent stage measurements using the model, the calibration can be rechecked infrequently to assess its stability.

The linear regression used here for the calibration does not substantially affect the qualitative performance results of the models. It simply scales all of the index discharges by the same amount so that they match the range of the true discharge. Nonlinear calibrations may be more appropriate in some systems (Ruhl and Simpson 2005), and these scale the discharges by amounts depending on the magnitude of the discharge, which could amplify or dampen the time series at high discharges. It is unlikely that these additional effects would substantially impact the performance of the k-means model or the Volterra series models, both of which are flexible enough to adapt to this additional nonlinearity.

### Low flows and missing data

When the stage in the creek is below the first cell of the ADCP profile, no valid velocity bins are recorded by the instrument. While the velocities at these stages can be fast, the flooded cross-sectional area of the channel is very small, so the true discharges are also small. We fill these missing discharges with zeros, and we estimate all of the models on these zero-filled discharge time series. This imputation is likely to bias our discharge estimates (Little and Rubin 2002), and it certainly prevents us from consistently estimating the discharge during these low-flow periods. Volumes exchanged during these periods are small relative to the entire tidal prism, so the imputation with zeros has little impact on the estimated water balance of the marsh. If one is not particularly interested in the exact discharge during these periods, the Boon, Volterra series and k-means model are all able to estimate zero discharges during these periods. These low flows during ebb tides, however, represent slow drainage out of the marsh and creek system and so have the potential to transport significant amounts of nutrients from the marsh (Gardner 1975; Fagherazzi et al. 2013). If it is important to capture these effects or to quantify the uncertainty that results from imputation, more sophisticated imputation of the discharge at low stages is possible (Hopke et al. 2001).

# Comments and recommendations

### A simplified method to compute tidal discharges from water levels

Based on the results presented herein, we suggest the following simplified method to estimate discharge in tidal channels from water stage using the threshold-based approximation to the k-means model. Choose a threshold stage that corresponds to the

565 elevation of the bank. If the left and right banks are asymmetric or there are multiple
566 steps up to the marsh platform, choose the lowest bank elevation. Segment the time series
567 into four groups: flood tide below the threshold, flood tide above the threshold, ebb tide
568 below the threshold and ebb tide above the threshold. The flood/ebb distinction can be
569 made quantitatively by taking differences between the current stage and the stage at the
570 previous time step. These differences will be positive on the flood tide and negative on
571 the ebb tide.

572 For each of the four groups of data, form a design matrix where each row represents a
573 data point and each column contains the stage data from the previous time steps. That is,
574 for row $i$, the first column contains the stage at time step $i$, $h_i$, the second
575 column contains $h_{i-1}$, the third column $h_{i-2}$ and so on. The number of columns,
576 $M$, should cover two whole tides. At the 10 minute sampling interval of the time
577 series presented here, this is approximately $M=150$ time steps, resulting in a design
578 matrix with 150 columns. If the time series is at a different sampling interval, change the
579 width of the design matrix accordingly.

580 One should now have a design matrix for each of the four time series segments $H_1$,
581 $H_2$, $H_3$ and $H_4$, and four vectors of discharge values $Q_1$, $Q_2$, $Q_3$ and
582 $Q_4$ each of which contains the corresponding discharge values for each of the data
583 points. The coefficients of the model are the four vectors $\beta_i=\left(H_i^T H_i\right)^{-1} H_i^T Q_i$ which
584 can be obtained with standard routines for linear regression. Once the four vectors of
585 coefficients are obtained, prediction of discharge at a new point proceeds by first
586 deciding to which of the four groups (high flood, low flood, high ebb, low ebb) the water

587 stage belongs. Each of the previous $M$ time steps of the stage is then multiplied by
588 each of the $M$ model coefficients of the corresponding group and added together to
589 provide an estimate of discharge.

590 **Model recommendations**

591 The complexity of estimating each of these models tracks closely their performance. The
592 linear, time-invariant model is a straightforward linear regression, but it performs the
593 worst (as measured by any of our error measures presented in Table 2). The Boon model
594 (as formulated here) requires a nonlinear least squares algorithm but does significantly
595 better. The k-means model has a mean squared error half that of the Boon model, but
596 requires some clustering either through k-means or the simplified threshold model
597 presented above. The Volterra model performs the best of all four models but requires a
598 computationally-intensive kernel regression. Choosing between the models is an exercise
599 in trading off complexity for predictive ability and requires a rigorously defined selection
600 criterion adapted to the particular application. We have used the mean squared error,
601 Nash-Sutcliffe efficiency and spectral flatness of residuals to argue that the cubic Volterra
602 series model with 25 hours of lagged stage observations performs the best of the four
603 models. However, each of these measures simply reflects the discrepancy between
604 modeled and observed instantaneous discharges, which may not be appropriate for all
605 applications. One could envision the integrated volume of water over a tide being more
606 important than the instantaneous discharge, in which case it might be worth selecting
607 model that slightly misestimates the discharge to get a more accurate estimate of the tidal
608 prism.

To help quantify the tradeoff between complexity and performance for applications, we have calculated the mean absolute percent error for each model as a function of stage (Fig. 7). We bin the stage into 50 cm bins and calculate the mean of the absolute value of the percent error between the modeled and estimated discharge within each bin. This gives some estimate of how far off one might expect to be when using each model to predict discharge over a certain range of stages. The general pattern follows our conclusions from the other measures of the model error with the Volterra series model performing the best, followed by k-means, Boon and the linear, time-invariant model. The Volterra series percent error is around 10-15% at all stages, while the k-means percent error ranges from around 20-30%. While the Boon model has a percent error around 50% at high and low stages, it is within one percent at stages just above the bankfull stage for our channel. If one is interested in estimating only the bankfull discharge in a channel, the Boon model performs just as well as the significantly more complex k-means model.

The k-means model, and especially the thresholded variation on the k-means model, represents, we believe, the best model for applications that need to estimate discharge from long-term records of stage such as biogeochemical and ecological investigations. It offers good estimation performance throughout a long time series, its estimation complexity comes from the selection of clusters, which can be well-approximated by the heuristic of a threshold, and it provides an appealing interpretation of the clusters in terms of flow regimes.

# Acknowledgements

This research was supported by the National Science Foundation (awards OCE1354251, OCE1354494, and OCE1238212). Data are publicly available through the Long Term Ecological Research (LTER) Network Data Portal at http://portal.lternet.edu. Code in the Julia language for estimating these models will be available at https://www.github.com/wkearn/TidalDischargeModels. We would like to thank Hillary Sullivan, Ian Craick and the students of the BU Marine Program for their help in collecting calibration data and Neil Ganju and two anonymous reviewers for their comments on a draft of this manuscript.

# Tables

640 **Table 1**: ADCP parameters

| Parameter | Value |
|---|---|
| Acoustic frequency | 2.0 MHz |
| Blanking distance | 10 cm |
| Cell size | 20 cm |
| Sampling interval | 10 minutes |

641

642 **Table 2**: Performance of the models

| Model | Mean squared error | Nash-Sutcliffe efficiency | Spectral flatness |
|---|---|---|---|
| Boon | 0.234 | 0.816 | 0.041 |
| LTI | 0.463 | 0.647 | 0.021 |
| Volterra | 0.025 | 0.980 | 0.273 |
| K-means | 0.118 | 0.910 | 0.257 |

643

# References


Aravkin, A. Y., J. V. Burke, and G. Pillonetto. 2013. Linear system identification using stable spline kernels and PLQ penalties. 52nd IEEE Conference on Decision and Control. doi:10.1109/cdc.2013.6760701

Bayliss-Smith, T., R. Healey, R. Lailey, T. Spencer, and D. Stoddart. 1979. Tidal flows in salt marsh creeks. Estuarine and Coastal Marine Science 9: 235–255. doi:10.1016/0302-3524(79)90038-0

Beven, K., and J. Davies. 2015. Velocities, celerities and the basin of attraction in catchment response. Hydrological Processes 29: 5214–5226. doi:10.1002/Hyp.10699

Blanton, J. O., G. Lin, and S. A. Elston. 2002. Tidal current asymmetry in shallow estuaries and tidal creeks. Continental Shelf Research 22: 1731–1743. doi:10.1016/S0278-4343(02)00035-3

Boon, J. D. 1975. Tidal discharge asymmetry in a salt marsh drainage system. Limnology and Oceanography 20: 71–80. doi:10.4319/lo.1975.20.1.0071

Botter, G., E. Bertuzzo, and A. Rinaldo. 2010. Transport in the hydrologic response: Travel time distributions, soil moisture dynamics, and the old water paradox. Water Resources Research 46: W03514. doi:10.1029/2009wr008371

Burnham, K. P., and D. R. Anderson. 2002. Model selection and multimodel inference, Springer.

663 Bühlmann, P. 2002. Bootstraps for time series. Statist. Sci. 17: 52–72.
664 doi:10.1214/ss/1023798998

665 Cai, W.-J. 2011. Estuarine and coastal ocean carbon paradox: CO2 sinks or sites of
666 terrestrial carbon incineration? Ann. Rev. Marine. Sci. 3: 123–145. doi:10.1146/Annurev-
667 Marine-120709-142723

668 Carey, J. C., and R. W. Fulweiler. 2014. Salt marsh tidal exchange increases residence
669 time of silica in estuaries. Limnology and Oceanography 59: 1203–1212.
670 doi:10.4319/lo.2014.59.4.1203

671 Chmura, G. L., S. C. Anisfeld, D. R. Cahoon, and J. C. Lynch. 2003. Global carbon
672 sequestration in tidal, saline wetland soils. Global Biogeochemical Cycles 17: 1111.
673 doi:10.1029/2002GB001917

674 Duarte, C. M., J. J. Middelburg, and N. Caraco. 2005. Major role of marine vegetation on
675 the oceanic carbon cycle. Biogeosciences 2: 1–8. doi:10.5194/Bg-2-1-2005

676 Fagherazzi, S. 2002. Basic flow field in a tidal basin. Geophysical Research Letters 29:
677 62-1 – 62-3. doi: 10.1029/2001GL013787

678 Fagherazzi, S., P. L. Wiberg, and A. D. Howard. 2003. Tidal flow field in a small basin.
679 Journal of Geophysical Research: Oceans 108: 16-1 – 16-10. doi: 10.1029/2002JC001340

680 Fagherazzi, S., M. Hannion, and P. D'Odorico. 2008. Geomorphic structure of tidal
681 hydrodynamics in salt marsh creeks. Water Resources Research 44: W02419.
682 doi:10.1029/2007wr006289

683 Fagherazzi, S., P. L. Wiberg, S. Temmerman, E. Struyf, Y. Zhao, and P. A. Raymond.
684 2013. Fluxes of water, sediments, and biogeochemical compounds in salt marshes.
685 Ecological Processes 2: 3. doi:10.1186/2192-1709-2-3

686 Franz, M. O., and B. Schölkopf. 2006. A unifying view of Wiener and Volterra theory and
687 polynomial kernel regression. Neural Computation 18: 3097–3118.
688 doi:10.1162/Neco.2006.18.12.3097

689 Ganju, N. K., M. L. Kirwan, P. J. Dickhudt, G. R. Guntenspergen, D. R. Cahoon, and K.
690 D. Kroeger. 2015. Sediment transport-based metrics of wetland stability. Geophysical
691 Research Letters 42: 7992–8000.

692 Ganju, N. K., N. J. Nidzieko, and M. L. Kirwan. 2013. Inferring tidal wetland stability
693 from channel sediment fluxes: Observations and a conceptual model. Journal of
694 Geophysical Research: Earth Surface 118: 2045–2058. doi:10.1002/jgrf.20143

695 Gardner, L. R. 1975. Runoff from an intertidal marsh during tidal exposure-recession
696 curves and chemical characteristics. Limnology and Oceanography 20: 81–89.
697 doi:10.4319/Lo.1975.20.1.0081

698 Harman, C. J. 2015. Time-variable transit time distributions and transport: Theory and
699 application to storage-dependent transport of chloride in a watershed. Water Resources
700 Research 51: 1–30. doi:10.1002/2014wr015707

701 Healey, R., K. Pye, D. Stoddart, and T. Bayliss-Smith. 1981. Velocity variations in salt
702 marsh creeks, norfolk, england. Estuarine, Coastal and Shelf Science 13: 535–545.
703 doi:10.1016/S0302-3524(81)80056-4

Hocking, R. R. 1976. The analysis and selection of variables in linear regression. Biometrics 32: 1–49.

Hopke, P. K., C. Liu, and D. B. Rubin. 2001. Multiple imputation for multivariate data with missing and below-threshold measurements: Time-series concentrations of pollutants in the arctic. Biometrics 57: 22–33. doi:10.1111/j.0006-341x.2001.00022.x

Kelley, C. T. 1999. Iterative methods for optimization, Society for Industrial & Applied Mathematics (SIAM).

Kennedy, E. J. 1984. Discharge ratings at gaging stations. U.S. Geological Survey Techniques of Water-Resources Investigations.

Little, R. J. A., and D. B. Rubin. 2002. Statistical analysis with missing data, 2nd ed. Wiley-Blackwell.

Ljung, G. M., and G. E. P. Box. 1978. On a measure of lack of fit in time series models. Biometrika 65: 297–303. doi:10.1093/biomet/65.2.297

Morris, J. T., P. V. Sundareshwar, C. T. Nietch, B. Kjerfve, and D. R. Cahoon. 2002. Responses of coastal wetlands to rising sea level. Ecology 83: 2869–2877. doi:10.1890/0012-9658(2002)083[2869:ROCWTR]2.0.CO;2

Mueller, D. S., C. R. Wagner, M. S. Rehmel, K. A. Oberg, and F. Rainville. 2009. Measuring discharge with acoustic doppler current profilers from a moving boat. U.S. Geological Survey Techniques; Methods.

Myrick, R. M., and L. B. Leopold. 1963. Hydraulic geometry of a small tidal estuary. US Geological Survey.

725 Pethick, J. 1980. Velocity surges and asymmetry in tidal channels. Estuarine and Coastal
726 Marine Science 11: 331–345. doi:10.1016/S0302-3524(80)80087-9

727 Pillonetto, G., and G. De Nicolao. 2010. A new kernel-based approach for linear system
728 identification. Automatica 46: 81–93. doi:10.1016/J.Automatica.2009.10.031

729 Rugh, W. J. 1981. Nonlinear system theory, Johns Hopkins University Press Baltimore.

730 Ruhl, C. A., and M. R. Simpson. 2005. Computation of discharge using the index-
731 velocity method in tidally affected areas. US Geological Survey.

732 Speer, P., and D. Aubrey. 1985. A study of non-linear tidal propagation in shallow
733 inlet/estuarine systems. Part II: Theory. Estuarine, Coastal and Shelf Science 21: 207–
734 224. doi:10.1016/0272-7714(85)90097-6

735 Tibshirani, R. 1996. Regression shrinkage and selection via the lasso. Journal of the
736 Royal Statistical Society. Series B (Methodological) 267–288.

737 Wold, S., A. Ruhe, H. Wold, and W. Dunn III. 1984. The collinearity problem in linear
738 regression. the partial least squares (pls) approach to generalized inverses. SIAM Journal
739 on Scientific and Statistical Computing 5: 735–743.

740 Xu, R., and D. Wunsch. 2009. Clustering, John Wiley & Sons.

741 Zou, H., and T. Hastie. 2005. Regularization and variable selection via the elastic net.
742 Journal of the Royal Statistical Society: Series B (Statistical Methodology) 67: 301–320.

# Figure legends

**Figure 1**: a) An aerial image (USGS, 2013) of the Sweeney Creek marsh. The red star is the location of the ADCP. The Rowley River is the large channel at the top of the image. b) The GPS cross section of the channel.

**Figure 2**: a) Velocities in the horizontal plane recorded by the Acoustic Doppler Current Profiler. The dominant direction of variability corresponds to the along-channel velocities. b) The true discharge obtained with a handheld flow meter plotted against the index discharge derived from the ADCP. The line represents the linear model $Q = 0.3477Q_i - 0.0416$ used to calibrate the index discharge ($Q_i$) to the true discharge ($Q$). c) Stage and discharge time series. The spring-neap tidal cycle over the course of the month results in nonstationarity in the discharge time series. d) An example stage-discharge relationship from a one-month ADCP record in Sweeney Creek, Rowley, MA. Note the bidirectionality and hysteresis in ebb and flood.

**Figure 3**: a) The hypsometric curve estimated in the Boon model. b) The impulse response estimated in the linear, time-invariant model. c) The first-order Volterra kernel is equivalent to a linear, time-invariant impulse response (top). The second-order kernel is a two-dimensional analogue of the impulse response. The distance along the x- and y-axes are the lags backwards in time for each of the directions of the impulse response. The color is the amplitude of the impulse response. d) The k-means model estimates $k$

764 impulse responses (top). Each impulse response is used to estimate from the
765 correspondingly colored point in the stage time series (bottom).

766

767 **Figure 4**: The modeled discharge plotted against the observed discharge. The line in each
768 plot is the one-to-one line.

769

770 **Figure 5**: The residual time series for each of the four classes of models: a) Boon, c)
771 Linear, time-invariant, e) Volterra series g) k-means. The power spectrum of the residual
772 time series for each of the four models b) Boon, d) Linear time-invariant, f) Volterra
773 series, b) k-means.

774

775 **Figure 6**: a) The unregularized impulse response for the linear, time-invariant model. b)
776 The regularized impulse response

777

778 **Figure 7**: Mean absolute percent error for each of the four models as a function of stage.
779 The solid blue line corresponds to the Boon model, the dashed red line to the linear, time
780 invariant model, the dotted green line to the Volterra series model and the dot-dashed
781 purple line to the k-means model.

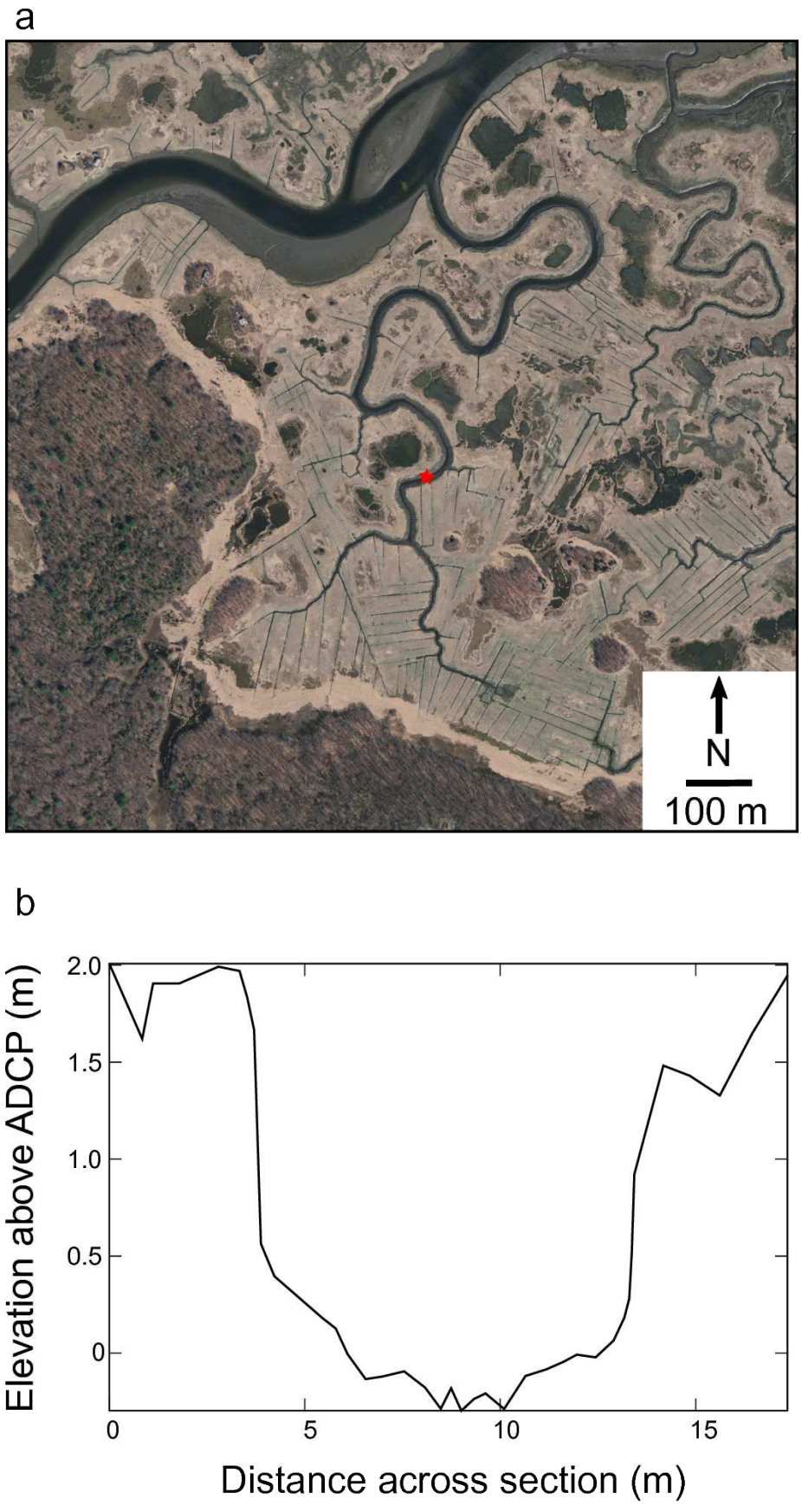
a
N
100 m
b
Elevation above ADCP (m)
2.0
1.5
1.0
0.5
0
0
5
10
15
Distance across section (m)

Figure 1:

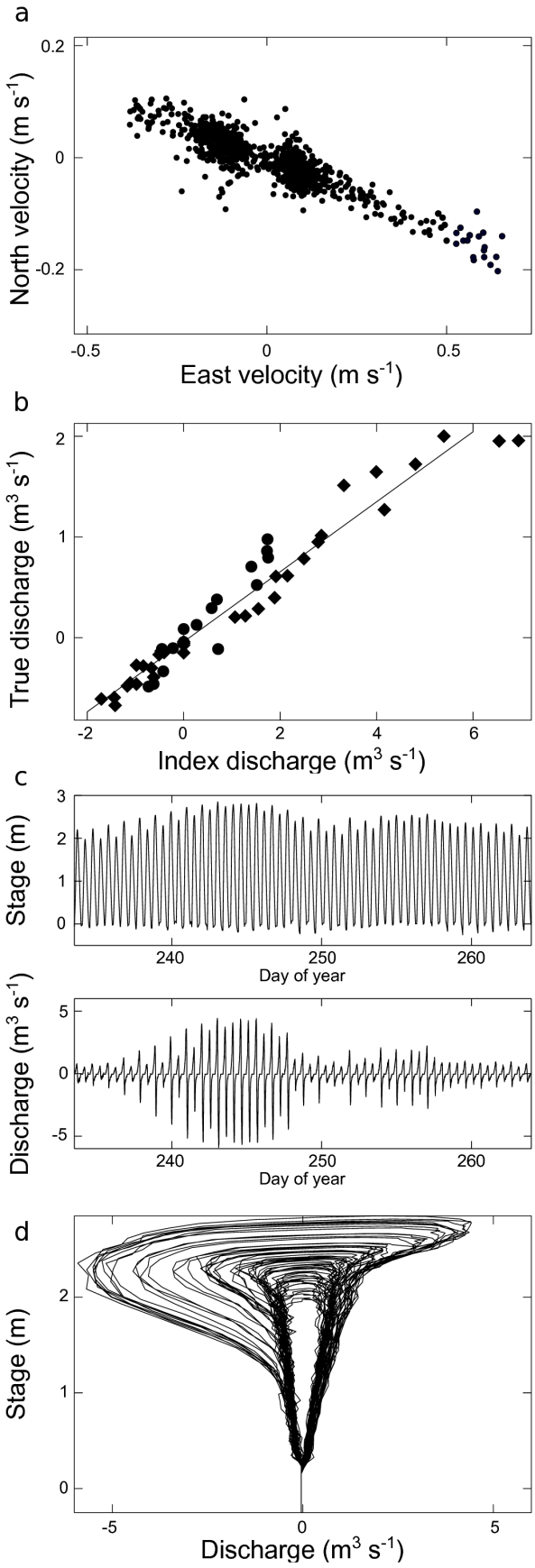
a
North velocity (m s-1)
East velocity (m s-1)
b
True discharge (m3 s-1)
Index discharge (m3 s-1)
c
Stage (m)
Day of year
Discharge (m3 s-1)
Day of year
d
Stage (m)
Discharge (m3 s-1)

Figure 2:

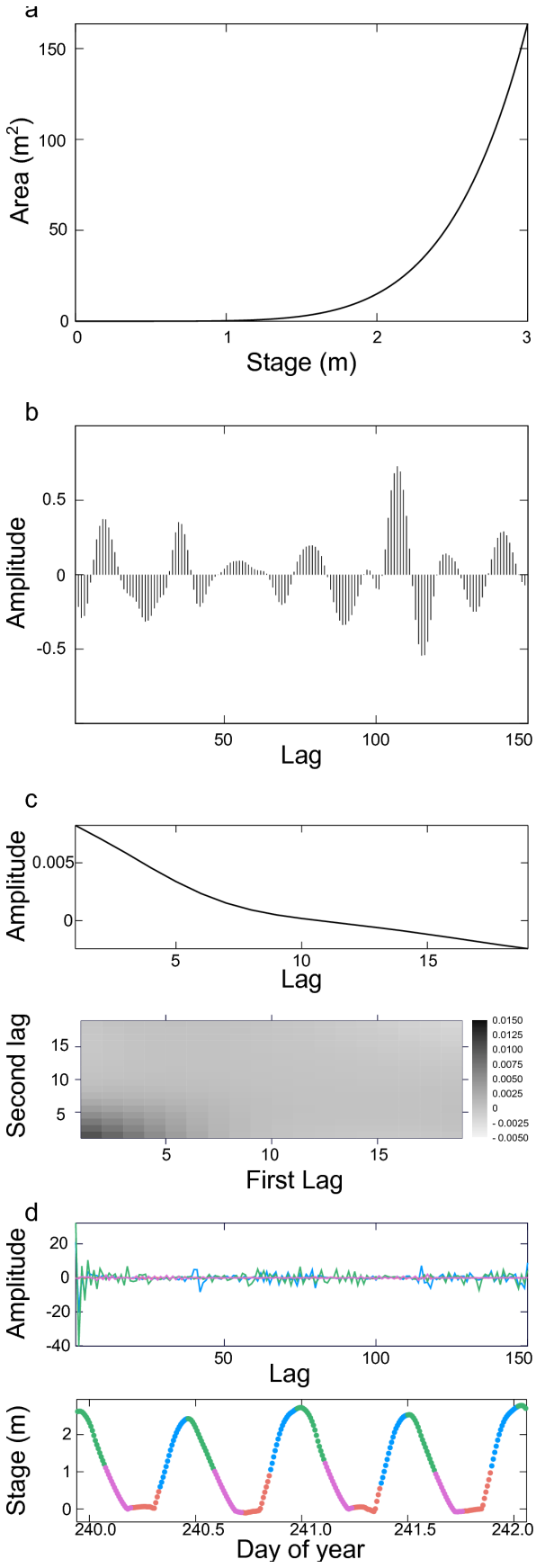
a
Area (m2)
Stage (m)
b
Amplitude
Lag
c
Amplitude
Lag
Second lag
First Lag
d
Amplitude
Lag
Stage (m)
Day of year

Figure 3:

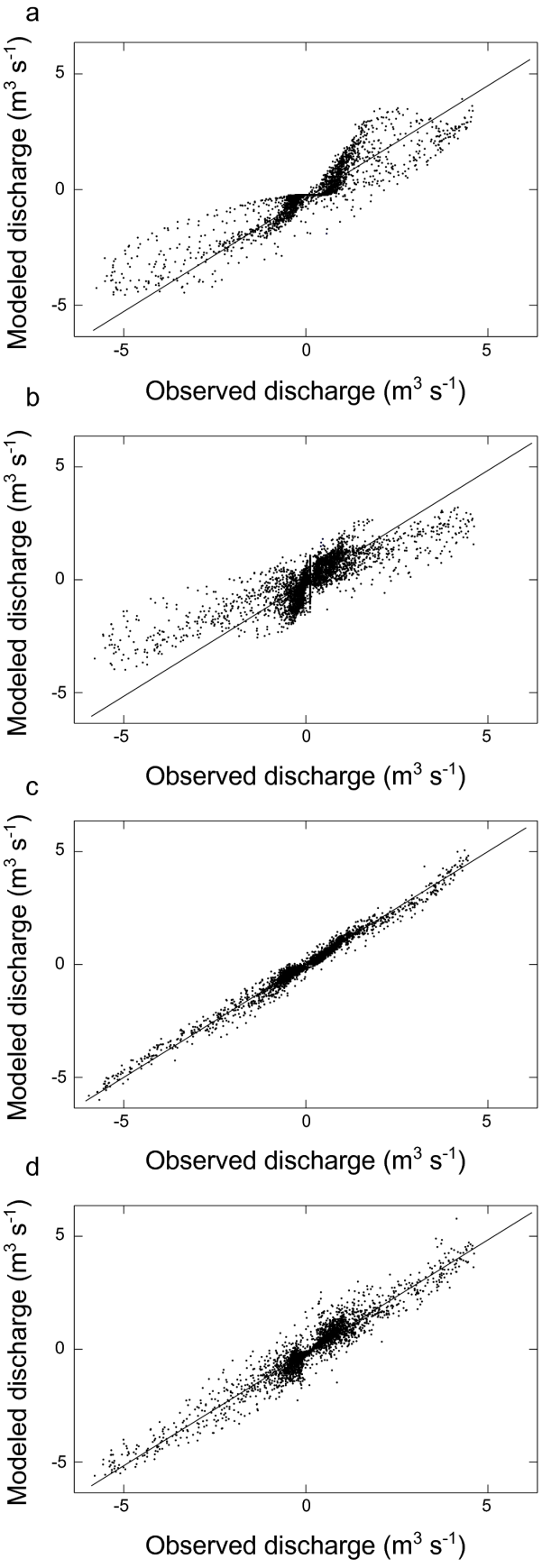


Figure 4:

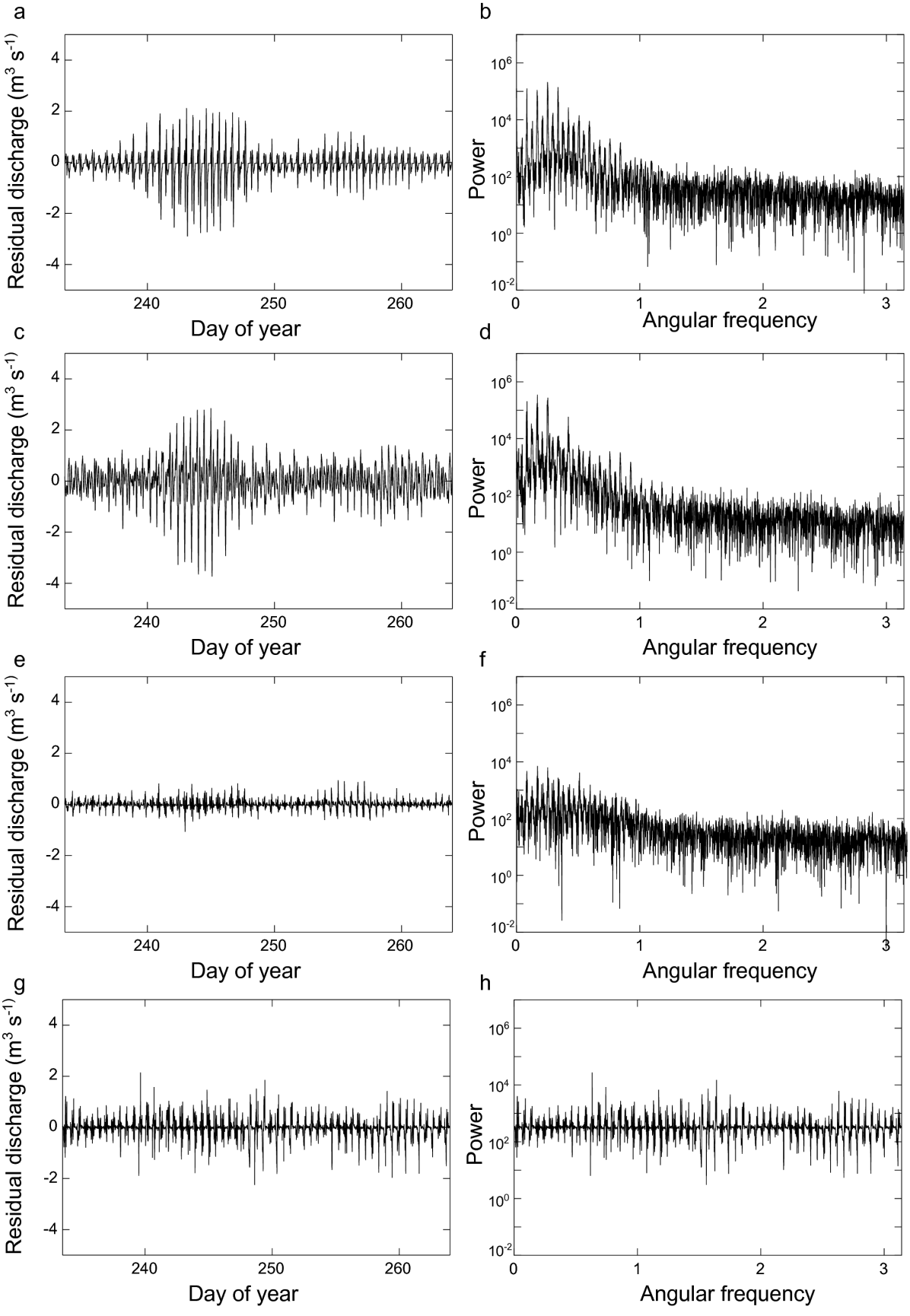
a
b
c
d
e
f
g
h
Residual discharge (m3 s-1)
Day of year
Power
Angular frequency
240
250
260
0
1
2
3
4
-2
-4
10-2
100
102
104
106

Figure 5:

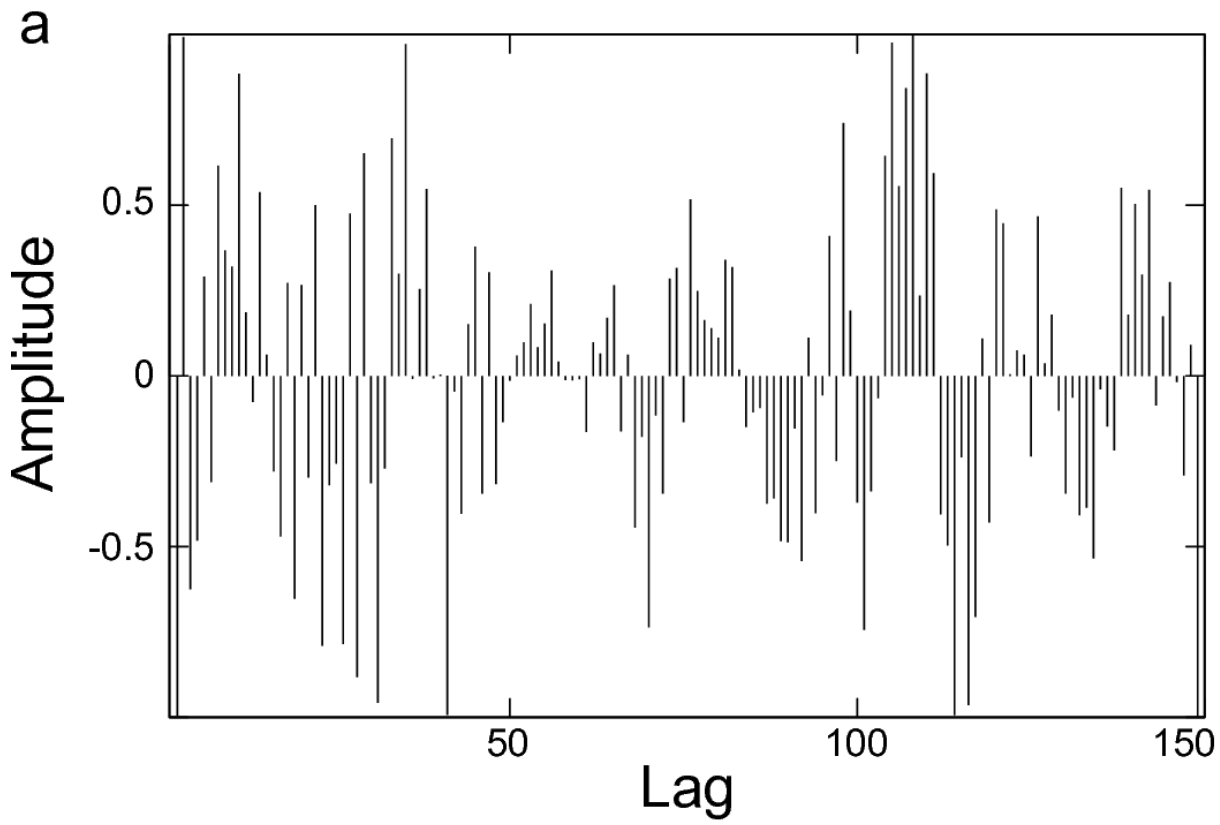
a
Amplitude
0.5
0
-0.5
50
100
150
Lag

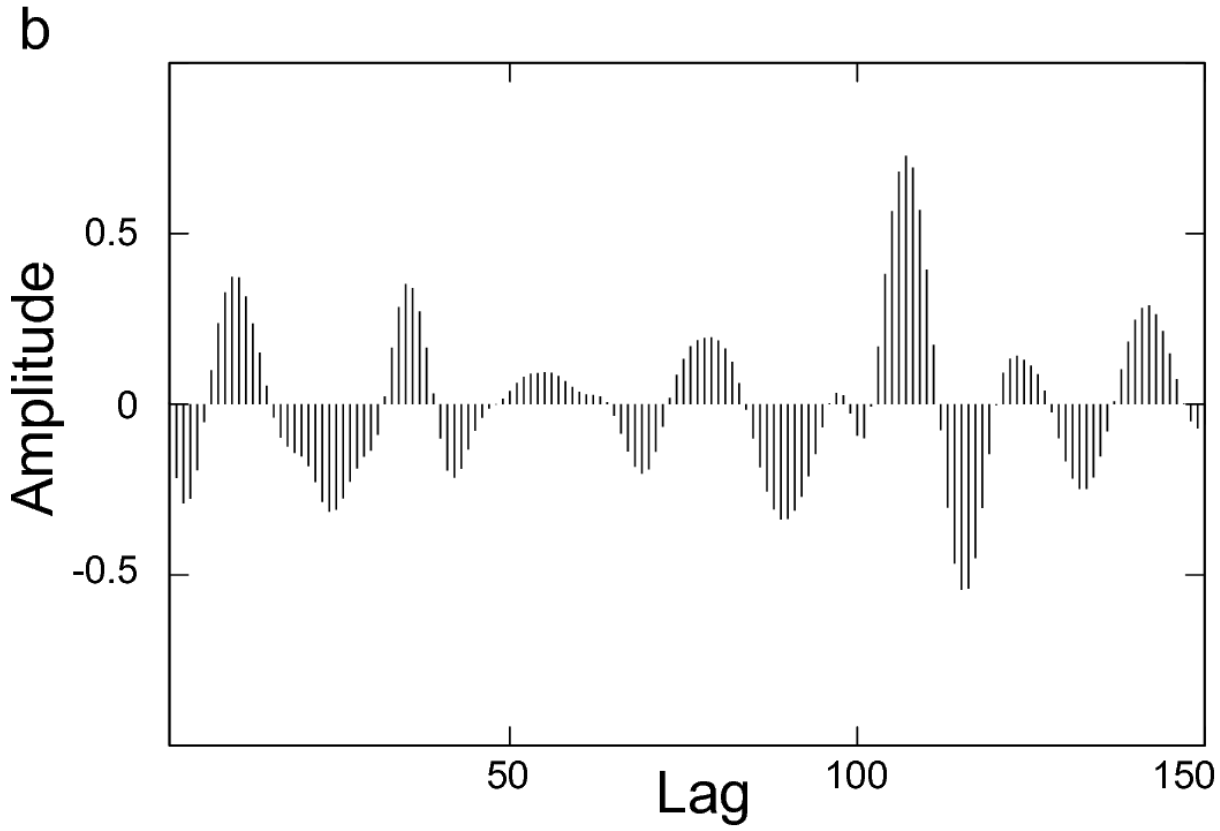
b
Amplitude
0.5
0
-0.5
50
100
150
Lag

Figure 6:

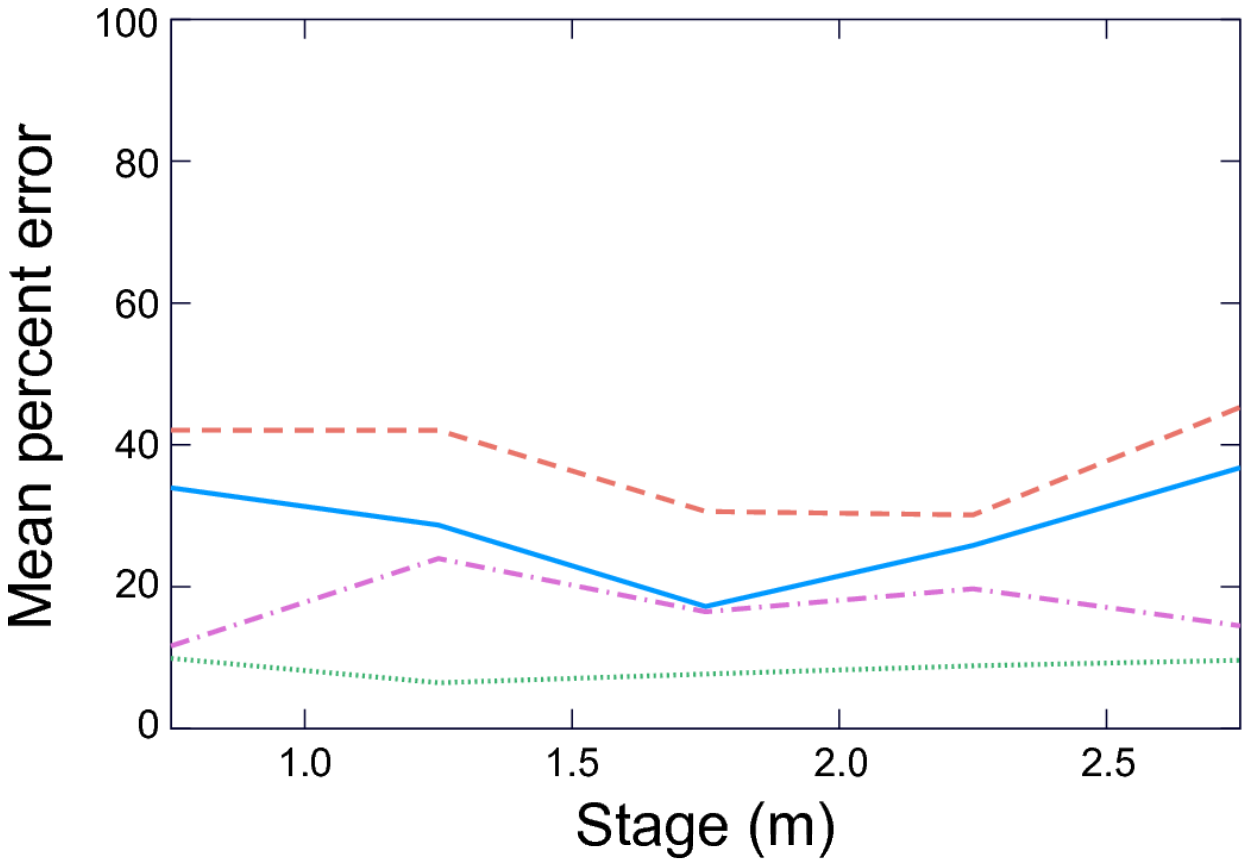


Figure 7: